Pseudo-Traveling-Wave Resonator With Magnetically Tunable Phase Gradient of Fields and Its Applications to Beam-Steering Antennas

Tetsuya Ueda, *Senior Member, IEEE*, Shintaro Yamamoto, Yuichi Kado, *Member, IEEE*, and Tatsuo Itoh, *Life Fellow, IEEE*

***Abstract*—A pseudo-traveling-wave resonator with magnetically tunable phase gradient of field distribution is investigated, and a new type of beam-steering antenna based on the resonator is experimentally demonstrated for the first time. It is a short-ended transmission-line resonator and is composed of a nonreciprocal phase-shift composite right/left-handed transmission line using a polycrystalline yttrium–iron–garnet rod. The resonator operates as zeroth-order resonator if there is no dc magnetic field, and the radiation beam directs to broadside. By increasing an externally applied dc magnetic field normal to the substrate, the effective dc magnetization in the ferrite increases under the unsaturated regime. The phase gradient of the field distribution along the resonator is then continuously increased. As a result, the radiation beam direction changes obliquely with respect to broadside. Continuous backfire-to-endfire beam steering with more than 40° was achieved with almost constant gain of 5 dBi. In addition, numerical simulation results show considerably high radiation efficiency of 85%–95%, and the measured beam angle and gain were found almost constant within the relative bandwidth of 2%.**

***Index Terms*—Beam steering, ferrite devices, leaky-wave antennas, metamaterials, periodic structures.**

I. Introduction

ZEROTH-ORDER resonators [1], [2] have been proposed and developed as one of transmission-line resonators, based on the concept of composite right/left-handed transmission lines (CRLHTLs) [2]–[4]. Resonant frequencies of conventional transmission-line resonators are determined by the length of the lines [5], whereas those of the zeroth-order resonators are not determined by the length itself, but by the configuration of the unit cell. Another interesting characteristic of the zeroth-order resonators is found in the field profiles with spatially uniform phase and amplitude along the line, which leads to applications in microwave filters, power dividers [6], [7], antennas [8]–[15], and oscillators [2]–[4].

Beam-steering leaky-wave antenna is another application of CRLHTL [16]–[27]. The beam direction can be continuously controlled from backfire through broadside to endfire by changing the operational frequency [16]–[23] or by electronically changing the configuration parameters [24]. However, the beam direction essentially fluctuates with the operation frequency even for electronically controlled beam scanning. Therefore, it restricts the use for communication applications with modulated signals. Another problem of conventional leaky-wave antennas is the low radiation efficiency due to existence of the nonradiated power consumption at the matched termination, especially for the compact type. There have been several proposals of power-recycling systems to improve the low-efficient antennas by using additional feedback systems [25]–[27].

Based on the concept of the CRLHTL, one of the authors proposed nonreciprocal components/devices, such as microwave edge-guided-mode isolators that are constructed by replacing a dielectric substrate of CRLH microstrip lines by a normally magnetized ferrite substrate [28]–[30]. We note that most microwave components/devices based on metamaterials, in general, utilize their attractive phase characteristics of guided waves, such as forward/backward wave propagation. Recently, from a phase-controlling point of view, another type of nonreciprocal transmission lines was proposed, which supports a dominant right-handed (RH) mode with positive refractive index in one direction of the transmitted power, and a dominant left-handed (LH) mode with negative refractive index in the opposite direction [31]–[34]. The transmission lines were implemented into nonreciprocal leaky-wave antennas with obliquely unidirectional beam radiation [31] and with the gain enhancement due to constructive interference between leaky waves from an incident wave and the reflected waves at the terminal [35] and also in pseudo-traveling-wave resonators with both terminals open or shorted permitting multiple reflections [36]. The pseudo-traveling-wave resonator is a new-type of transmission-line resonator and has the field profiles with the uniform magnitude and gradient of the phase distribution along the resonator. We labeled it with "pseudo" because it is not a conventional pure traveling-wave resonator in that the transmitted power flow on the resonator for an ideal case without any losses vanishes after the cancellation due to

Manuscript received March 19, 2012; revised June 15, 2012; accepted June 17, 2012. Date of publication July 27, 2012; date of current version September 27, 2012. This work was supported in part by the Japan Society for the Promotion of Science (JSPS) under KAKENHI Grant 23560454 and by the Ministry of Education, Culture, Sports, Science and Technology (MEXT) under KAKENHI Grant 22109002.

T. Ueda, S. Yamamoto, and Y. Kado are with the Department of Electronics, Kyoto Institute of Technology Kyoto 606-8585, Japan (e-mail: ueda@kit.ac.jp; shintaro0902soccer@gmail.com; kado@kit.ac.jp).

T. Itoh is with the Department of Electrical Engineering, University of California at Los Angeles, Los Angeles, CA 90095-1594 USA (e-mail: itoh@ee.ucla.edu).

Color versions of one or more of the figures in this paper are available online at http://ieeexplore.ieee.org.

Digital Object Identifier 10.1109/TMTT.2012.2207737

multiple reflections at the terminals. The phase gradient of field distribution depends on the applied dc magnetic field and magnetization in the ferrite. Recently the pseudo-traveling-wave resonator is implemented into beam-scanning antennas [37] and beam-steering capability was numerically demonstrated by changing the applied dc magnetic field. However, numerical results were shown only for two cases: one without dc magnetic field, i.e., zeroth-order resonator antenna, and another case with saturated magnetization in the ferrite materials. Under the unsaturated magnetization regime for small externally applied dc field, nonreciprocal leaky-wave radiation from CRLHTL was investigated [38], but the resonator and the tunable phase gradient have not been investigated in detail.

In this paper, the pseudo-traveling-wave resonator is investigated mainly experimentally under the unsaturated magnetization regime, and the new type of beam-steering antenna based on the resonator is demonstrated for the first time. It is a short-ended transmission-line resonator and is composed of a nonreciprocal phase-shift CRLH microstrip line using polycrystalline yttrium–iron–garnet (YIG) rod. The resonator operates as a zeroth-order resonator if there is no external dc magnetic field, and the radiation beam from the resonator directs to broadside. By increasing an externally applied dc magnetic field normal to the substrate, the effective dc component of magnetization in the ferrite increases under the unsaturated region. The phase gradient of the field distribution along the resonator is then also enhanced. As a result, the radiation beam direction changes obliquely with respect to broadside. Continuous backfire-to-endfire beam steering with more than 40° was demonstrated with almost constant gain of 5 dBi. In addition, it is verified from numerical simulation that the proposed beam-steering antenna has considerably high radiation efficiency of 85%–95% because the resonant system in the antenna corresponds to an efficient power-recycling system. Finally, robustness of the beam angle against modulated signals is also discussed with comparison to conventional leaky-wave antennas, and the measured beam angle and gain were found almost constant within the relative bandwidth of 2%.

II. Basic Concept of Nonreciprocal CRLHTL and Pseudo-Traveling-Wave Resonator

A. Geometry and Equivalent Circuit Model for CRLHTL

Simplified equivalent-circuit models for a nonreciprocal phase-shift CRLHTL employed in the proposed resonator, the T-type unit cell, and schematic of the dispersion curves are illustrated in Fig. 1 [33]. The unit cell is composed of two transmission-line arm sections with nonreciprocal phase characteristics and series-capacitive and shunt-inductive elements. Quantities β_p and β_m in Fig. 1(a) and (b) denote phase constants for forward and backward propagation directions in the transmission-line arm section, respectively, and Z_p and Z_m denote the corresponding characteristic impedances. In Fig. 1(c) and (d), the dispersion curves for the nonreciprocal CRLHTL are shown. Fig. 1(c) and (d) denote the unbalanced and balanced cases with and without bandgap between upper and lower branches,

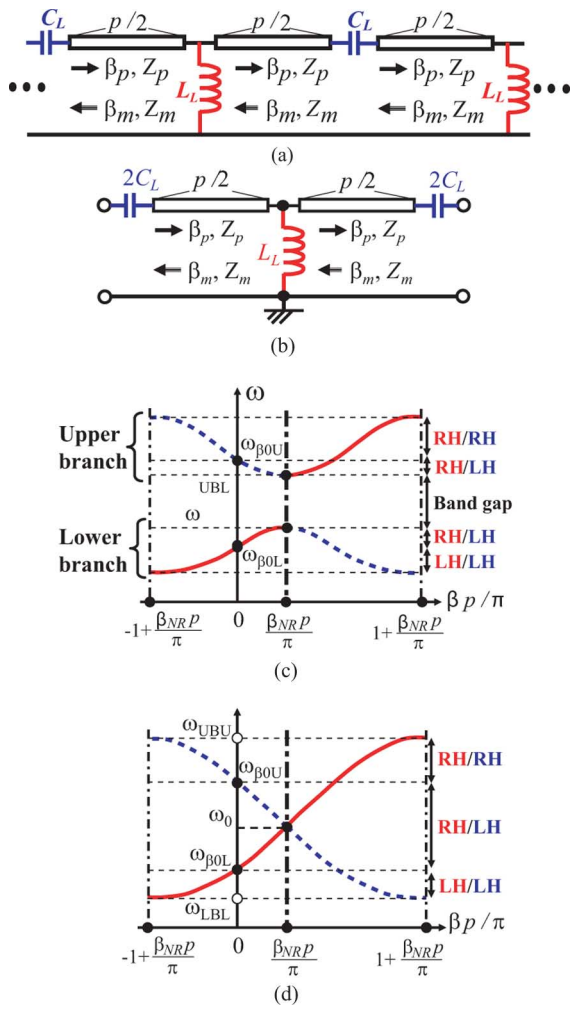

Fig. 1. Schematic of equivalent-circuit models: (a) for nonreciprocal CRLHTL and (b) for the T-type unit cell. Schematic of dispersion diagram: (c) for the unbalanced case with a bandgap between upper and lower branches and (d) for the balanced case without a bandgap.

respectively. As shown in Fig. 1(c) and (d), the dispersion curves of the dominant CRLH modes in the nonreciprocal CRLHTL has unique characteristics with a displacement of the symmetric axis originally aligned to the frequency axis to the left or right by the difference of phase constants between two propagation directions $\beta_{\mathrm{NR}} = (\beta_p - \beta_m)/2$ [31]. As a result, the nonreciprocal CRLHTL supports a dominant RH mode in a direction of the transmitted power and a dominant LH mode in the opposite direction along the line within the specific frequency region from $\omega_{\beta 0L}$ to $\omega_{\beta 0U}$ [31].

The practical geometry of the CRLHTL is shown in Fig. 2. The basic configuration is the same as in [33], [34], [36], and [37]. Series lumped capacitors and shorted inductive stubs are periodically inserted in a center microstrip line to achieve negative effective permeability and permittivity. A normally magnetized ferrite rod is embedded in the dielectric substrate just below the center microstrip, as shown in Fig. 2(b). The insertion of stubs are made only one side of the center microstrip edges in order to form an asymmetric geometry with respect to the plane including the propagation direction and the dc magnetization, leading to the nonreciprocal transmission

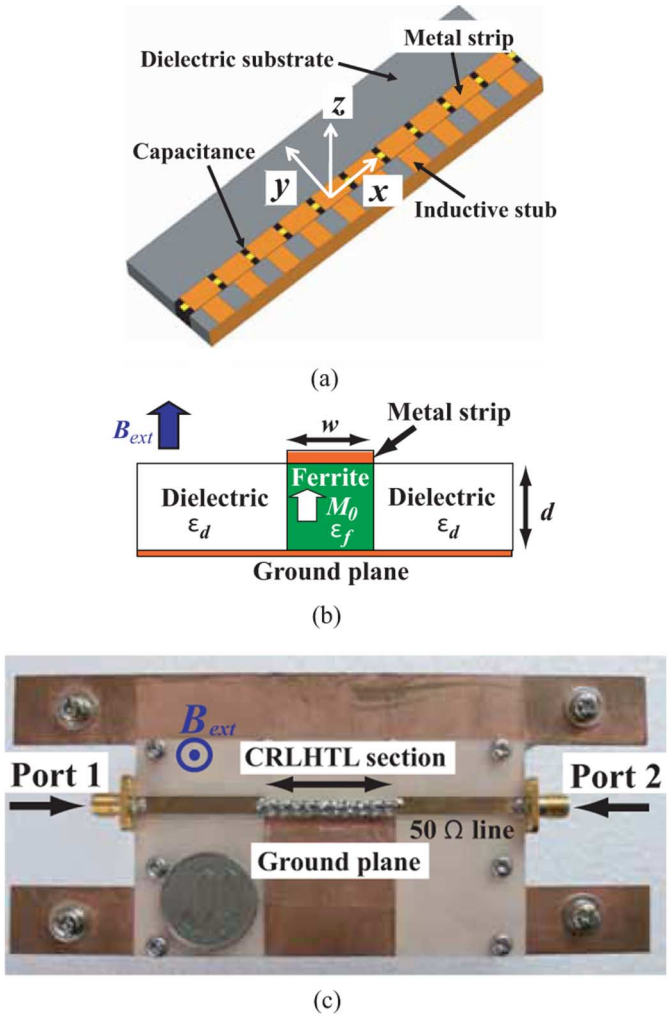

Fig. 2. Geometry of designed nonreciprocal CRLHTL and photo of the prototype. (a) Perspective view. (b) Cross section of center strip. (c) Photograph of top view of the fabricated CRLH line.

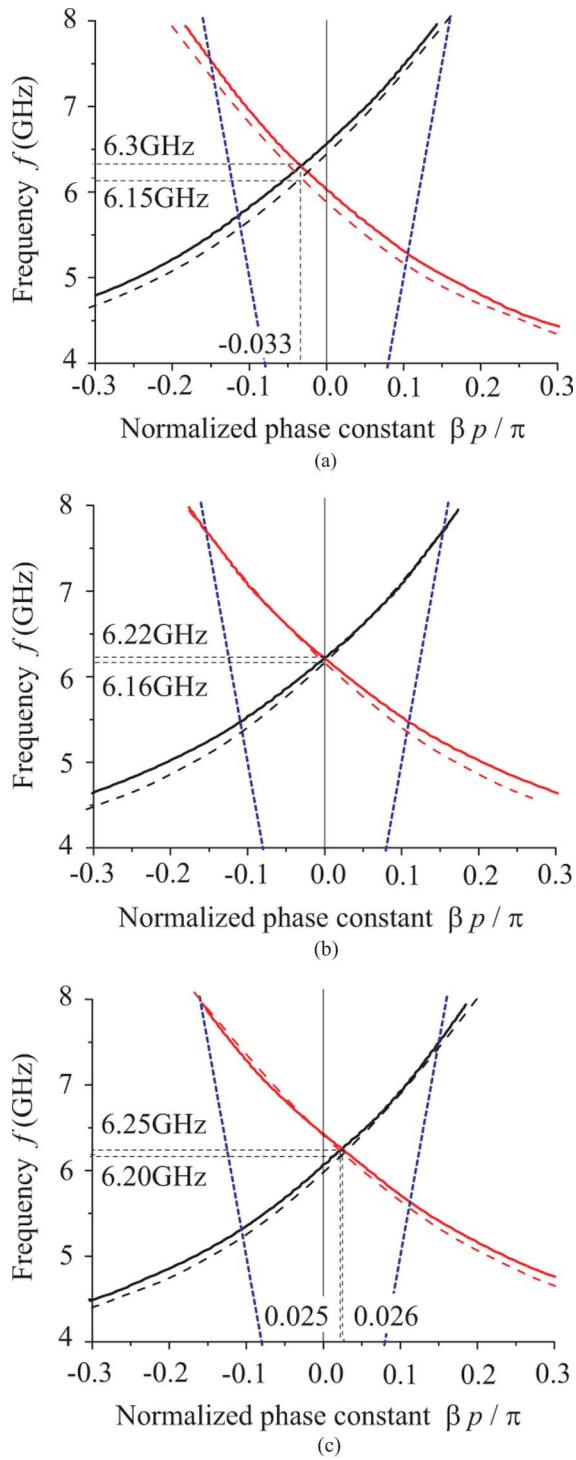

Fig. 3. Dispersion diagram estimated from phase of measured and simulated transmission coefficients. Solid and broken lines represent measured and simulated results, respectively. (a) $B_{\rm ext} = -55$ mT. (b) $B_{\rm ext} = 0$ mT. (c) $B_{\rm ext} = 34.5$ mT.

characteristics, as shown in Fig. 1(c) and (d). For the specific geometry in Fig. 2, the phase nonreciprocity $\beta_{\rm NR}$ in Fig. 1 is proportional to effective dc magnetization M_0 in the ferrite rod, as will be shown later. This ferrite-rod-embedded structure is employed because the insertion loss and the nonreciprocity in the magnitude of transmission coefficients are relatively small, whereas the nonreciprocal phase characteristics are still significant.

In what follows, we consider polycrystalline YIG as the soft ferrite, and polystyrene as the dielectric substrates. Since the polycrystalline YIG shows significantly large magnetic loss below 4.5 GHz without externally applied dc magnetic field in our experimental setup, the operational frequencies are set to around 6 GHz to avoid significant insertion loss.

The various configuration parameters designed in the numerical simulation are as follows; dimension of the ferrite rod is 1.6 mm×1.6 mm×30 mm, the relative permittivity of the ferrite rod and the dielectric substrates are $\varepsilon_f = 14.5$ and $\varepsilon_d = 2.62$, respectively. Dielectric loss tangents of the ferrite and dielectric materials are $\tan\delta_f = 0.0001$ and $\tan\delta_d = 0.0014$, respectively. Both thickness of the substrate and strip width of the center microstrip line are $w = d = 1.6$ mm. The length of the unit cell is $p = 3$ mm, and the total number of unit cells in the CRLHTL section is ten. The inserted series capacitance is $C = 0.4$ pF. The inserted shunt inductive stub is composed of a shorted microstrip line with the width of 1.5 mm and the length of 2.0 mm. Conductors employed are assumed to be copper with conductivity $\sigma = 5.8\times10^7$ S/m. The photograph of the top view

of the fabricated CRLHTL for measurement of the transmission characteristics is shown in Fig. 2(c).

In Fig. 3, dispersion diagrams of the fabricated nonreciprocal phase shift CRLHTL are plotted with solid lines as a function of the externally applied dc magnetic field. The phase constant in Fig. 3 was converted from the phase of measured S-parameters. The dc magnetic field in the experiment was varied from $B_{\rm ext} = -55$ mT through 0 to 110 mT by mechanically changing a distance between the CRLH line and a permanent magnet. Dimension of the magnet is 60 mm $\times$ 20 mm $\times$ 10 mm, and was placed below the ground plane. The applied dc field distribution in the region of interest to be inserted with the ferrite rod was measured without the insertion. The distribution was found almost uniform in the longitudinal direction and the representative values given in the paper were measured at the position where the center of the ferrite rod would be located. It is noted that the measured range of the external dc magnetic fields is insufficient for magnetization in the ferrite rod to be saturated. Since it is difficult to analytically treat behavior of the unsaturated magnetization in the ferrite, the effective magnetization was numerically estimated by comparing the measured nonreciprocal transmission characteristics and the simulation results under the assumption of uniform distribution of the magnetization. The magnetic loss of the ferrite used in the numerical simulation was $\mu_0 \Delta H = 5$ mT. The internal dc magnetic field used in the simulation was set to zero for simplicity since a further increase in the internal dc field does not change phase nonreciprocity so much, but leads to deviation from the measure transmission characteristics. The obtained relation among the measured external dc magnetic field, effective magnetization extracted, and the phase nonreciprocity is shown in Fig. 4. It is found from Fig. 4 that both the effective magnetization and phase nonreciprocity are approximately proportional to the applied dc magnetic field for the external dc magnetic field less than 50 mT. The simulated nonreciprocal dispersion curves adjusted to the measurement are also plotted with broken lines in Fig. 3. It is found from Fig. 3 that the measured frequency at the intersection of nonreciprocal RH and LH modes in the dispersion curves is relatively stable with deviation of the order of several dozen megahertz against small variation of the externally applied dc field. In what follows, we utilized the extracted effective magnetization to design and estimate the performance of pseudo-traveling-wave resonators and the antennas based on the nonreciprocal CRLHTL.

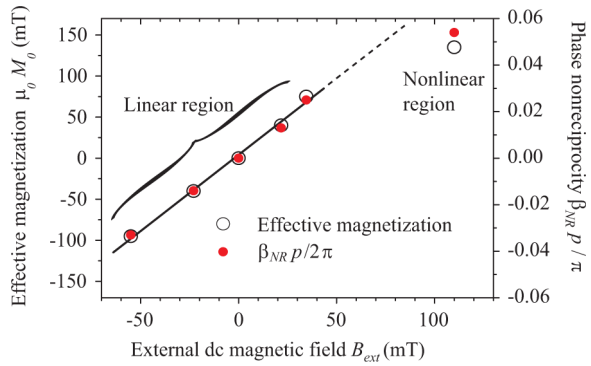

Fig. 4. Externally applied dc magnetic field versus effective magnetization and phase nonreciprocity.

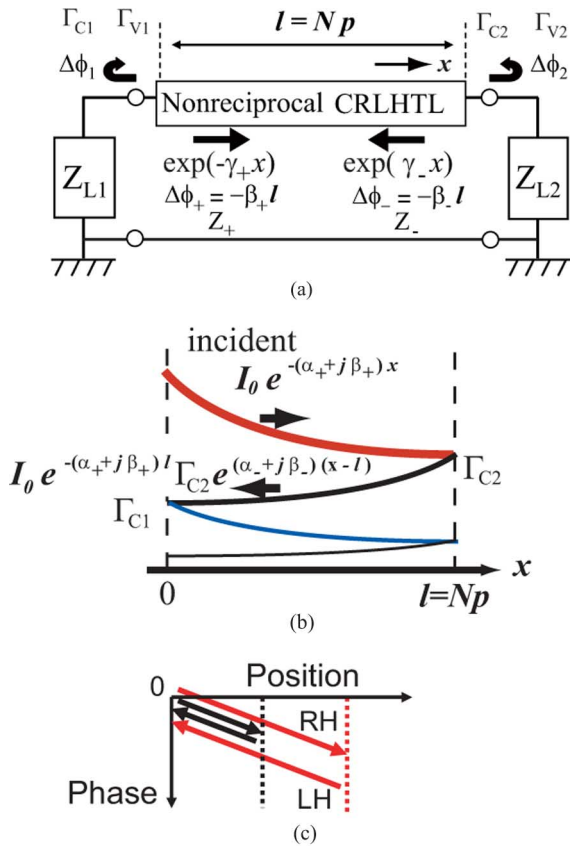

Fig. 5. Pseudo-traveling-wave resonator. (a) Equivalent-circuit model. (b) Current distribution. (c) Automatic phase matching condition independently of resonator's size.

The propagation constant $\gamma_+ = \alpha_+ + j\beta_+$ and $\gamma_- = \alpha_- + j\beta_-$ have been defined in Fig. 5 with the corresponding attenuation constant α_+ and α_-. The current distribution on the resonator can be expressed with multiple reflections of an incident wave at the terminals, as shown in Fig. 5(b), and the total current distribution is given by

$$\begin{aligned} I(x) &= I_0 e^{-(\alpha_+ + j\beta_+)x} + I_0 e^{-(\alpha_+ + j\beta_+)l} \\ &\quad \cdot \Gamma_{C2} e^{(\alpha_- + j\beta_-)(x-l)} + I_0 e^{-(\alpha_+ + j\beta_+)l} \\ &\quad \cdot \Gamma_{C2} e^{-(\alpha_- + j\beta_-)l} \cdot \Gamma_{C1} e^{-(\alpha_+ + j\beta_+)x} \\ &\quad + I_0 e^{-(\alpha_+ + j\beta_+)l} \cdot e^{-(\alpha_- + j\beta_-)l} \\ &\quad \cdot \Gamma_{C1} e^{-(\alpha_+ + j\beta_+)l} \cdot \Gamma_{C2} e^{(\alpha_- + j\beta_-)(x-l)} + \cdots \\ &= \frac{I_0 e^{-\gamma_+ l}}{1 - \Gamma_{C1}\Gamma_{C2} e^{-\gamma_{\rm sum} l}} [e^{-\gamma_+(x-l)} + \Gamma_{C2} e^{\gamma_-(x-l)}] \end{aligned} \quad (1)$$

B. Pseudo-Traveling-Wave Resonator

In this section, we discuss resonant condition and field profiles on the pseudo-traveling-wave resonator. In Fig. 5, the equivalent-circuit model, schematic of the current distribution along the CRLH section with the length of $l = Np$, and the phase matching condition are illustrated. The quantity N denotes the number of the unit cells. In Fig. 5(a), the quantities β_+ and β_- denote phase constants of these dominant CRLH modes, whose signs are taken so that the direction of the transmitted power is positive.

with

$$\begin{aligned}\gamma_{\rm sum} &= \alpha_{\rm sum} + j\beta_{\rm sum}\\ \alpha_{\rm sum} &= \alpha_+ + \alpha_-\\ \beta_{\rm sum} &= \beta_+ + \beta_-\end{aligned} \tag{2}$$

where Γ_{C1} and Γ_{C2} in (1) denote current reflection coefficients at Terminal 1 and 2, respectively. In the same manner, the voltage distribution is given by

$$V(x) = \frac{Z_+ I_0 e^{-\gamma_+ l}}{1-\Gamma_{V1}\Gamma_{V2}e^{-\gamma_{\rm sum} l}}[e^{-\gamma_+(x-l)} + \Gamma_{V2}e^{\gamma_-(x-l)}] \tag{3}$$

where Γ_{V1} and Γ_{V2} denote the corresponding voltage reflection coefficients at Terminal 1 and 2, and are related to current reflection coefficients with

$$\Gamma_{V1} = -\frac{Z_+}{Z_-}\Gamma_{C1} \quad \Gamma_{V2} = -\frac{Z_-}{Z_+}\Gamma_{C2}.$$

The quantities Z_+ and Z_- represent Bloch impedance of the nonreciprocal CRLHTL in the positive and negative x-direction. It is noted that the relation $\Gamma_{C1}\Gamma_{C2} = \Gamma_{V1}\Gamma_{V2}$ always holds. From (1) and (3), the transmitted power distribution along the resonator can also be formulated and given by (4), shown at the bottom of this page. The resonant condition is satisfied in a situation where the magnitude of denominator in (1) or (3) takes the minimum, and we have

$$\begin{aligned}&1-\Gamma_{C1}\Gamma_{C2}e^{-\gamma_{\rm sum} l}\\ &\quad = 1-|\Gamma_{C1}||\Gamma_{C2}|e^{-\alpha_{\rm sum} l}e^{-\beta_{\rm sum} l+(\Delta\phi_1+\Delta\phi_2)}\\ &\quad \cong 0\end{aligned}$$

i.e.,

$$\begin{cases} -(\beta_+ + \beta_-)l + (\Delta\phi_1 + \Delta\phi_2) = 2m\pi\\ |\Gamma_{C1}||\Gamma_{C2}|e^{-\alpha_{\rm sum} l} \cong 1\end{cases} \tag{5}$$

where $\Delta\phi_1$ and $\Delta\phi_2$ denote the phase shift due to reflection at terminals 1 and 2, and m is the integer. The sum of the phase shift $\Delta\phi_1 + \Delta\phi_2$ can be neglected for open- or short-end cases. When the relation

$$\beta_+ + \beta_- = 0 \tag{6}$$

holds in (5), the resonant condition is independent of the resonator's size l and is automatically satisfied with $m = 0$ [36]. Fig. 5(c) shows the automatic phase-matching condition describing the phase distribution for traveling waves experiencing round trip on the resonator. The phase of an incident forward wave mode propagating to the right is delayed, whereas the phase of the backward wave mode that is reflected at the terminal and going back to the left gets advanced. When both gradients of the phase distribution are exactly the same, the total phase shift always vanishes to achieve the resonant condition. In what follows, we consider short-ended resonators. For simplified cases with the relation (6), $\alpha_+ = \alpha_-$, $Z_+ = Z_-$, and $\Gamma_{C1} = \Gamma_{C2} \sim 1$, or $\Gamma_{V1} = \Gamma_{V2} \sim -1$, (1), (3), and (4) are reduced to

$$I(x) = \frac{2I_0 e^{-\gamma_+ l}}{1-|\Gamma_{C2}|^2 e^{-2\alpha_+ l}}\cosh[\alpha_+(x-l)]\, e^{-j\beta_+(x-l)} \tag{7}$$

$$V(x) = \frac{2Z_+ I_0 e^{-\gamma_+ l}}{1-|\Gamma_{V2}|^2 e^{-2\alpha_+ l}}\sinh[\alpha_+(x-l)]\, e^{-j\beta_+(x-l)} \tag{8}$$

and

$$P(x) = \frac{-Z_+|I_0|^2 e^{-2\alpha_+ l}}{\left(1-|\Gamma_{C2}|^2 e^{-2\alpha_+ l}\right)^2}\sinh[2\alpha_+(x-l)]. \tag{9}$$

The above assumption of reciprocal characteristic impedance $Z_+ = Z_-$ approximately holds when we consider low-loss nonreciprocal transmission lines, as confirmed by the numerical simulation. Therefore, under the condition that a product of the attenuation constant and the total length of the resonator satisfies $|\alpha_+ l| \ll 1$, the current distribution along the resonator has almost uniform magnitude and linearly varying phase distribution. On the other hand, in that case, the transmitted power distribution on the resonator in (9) could be cancelled by the multiple reflections.

In Fig. 6, a practical configuration of the present pseudo-traveling-wave resonator is shown. The short-ended condition of the CRLHTL section is realized by using an open-ended quarter-wavelength transmission line as the reflectors, as shown in Fig. 6(a) and (b). The feed line is inserted on one of the finite-length transmission line sections in the reflectors so that the input impedance is almost 50 Ω. In Fig. 6(c), a photograph of the prototype resonator is shown. The feed lines that were used for connection to ports 1 and 2 in Fig. 2(c) have been removed in the circuit of Fig. 6(c).

Measured return loss, operational frequency, and the -10-dB bandwidth satisfying the voltage standing-wave ratio (VSWR) less than 2 are shown in Fig. 7 along with the numerical simulation results. The internal dc magnetic field and effective magnetization used in the numerical simulation have been kept the same as in Fig. 3. In Fig. 7(a), the measured resonant frequency is 6.12 GHz and the simulated is 6.15 GHz, and both were found to be lower than the frequencies estimated from dispersion curves in Fig. 3 due to an insufficient number of cells, as can be confirmed from further numerical simulation with larger numbers showing their good agreement. It is found from Fig. 7(b) that the measured resonant frequency is

$$P(x) = \frac{1}{2}\,V\,I^* = \frac{1}{2}\cdot\frac{|I_0|^2 e^{-2\alpha_+ l}}{|1-\Gamma_{C1}\Gamma_{C2}\,e^{-\gamma_{\rm sum} l}|^2}\times\left[Z_+\,e^{-2\alpha_+(x-l)} + Z_-\,e^{2\alpha_-(x-l)} + 2{\rm Im}(Z_+\Gamma_{C2}^*\,e^{(\gamma_-^*-\gamma_+)(x-l)})\right] \tag{4}$$

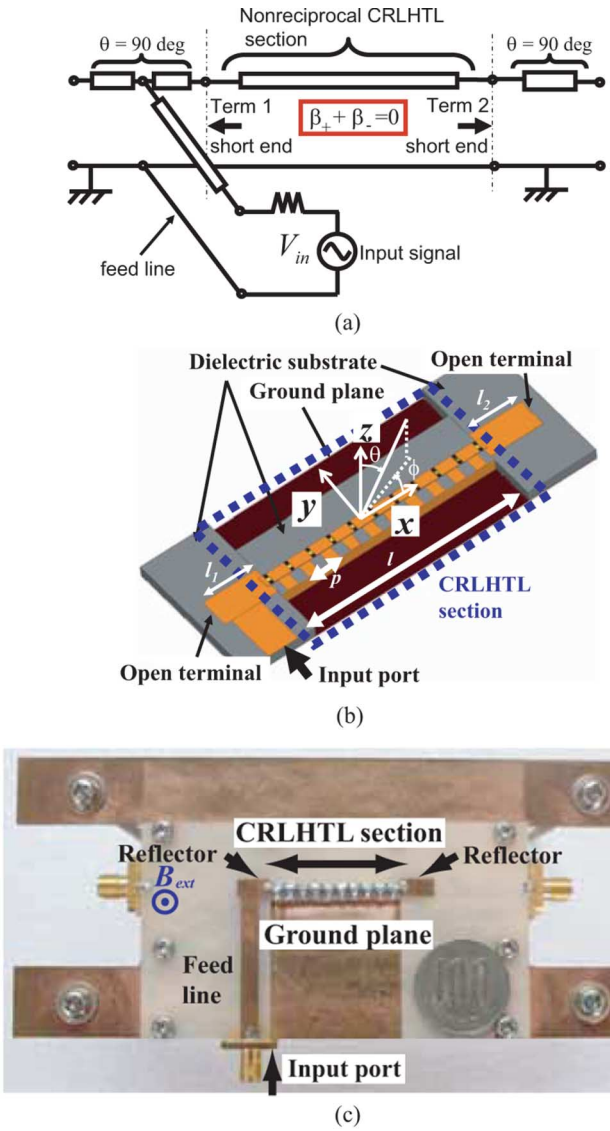

Fig. 6. Geometry of designed prototype pseudo-traveling-wave- resonator antenna. (a) Equivalent circuit. (b) Perspective view. (c) Photograph of the prototype resonator.

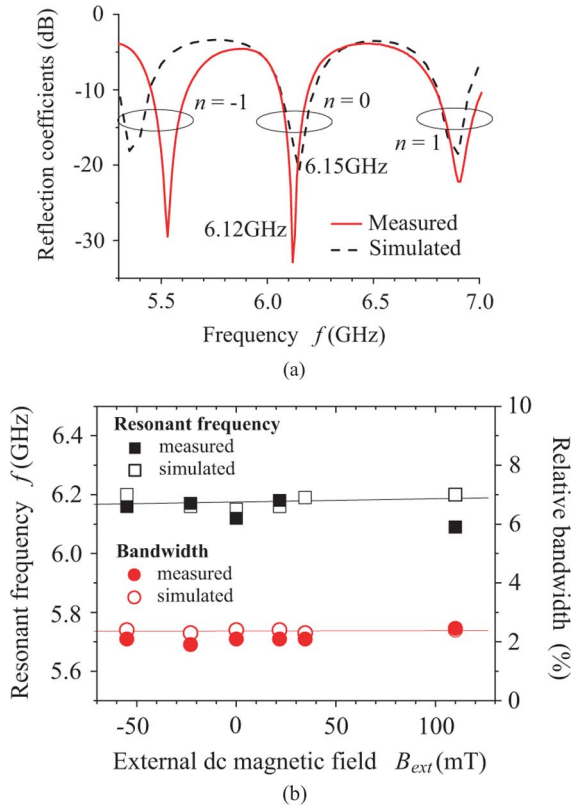

Fig. 7. Simulated and measured resonant characteristics of pseudo-traveling-wave resonator. (a) Reflection coefficients without dc magnetic field. (b) Resonant frequencies and bandwidths as a function of the applied dc field.

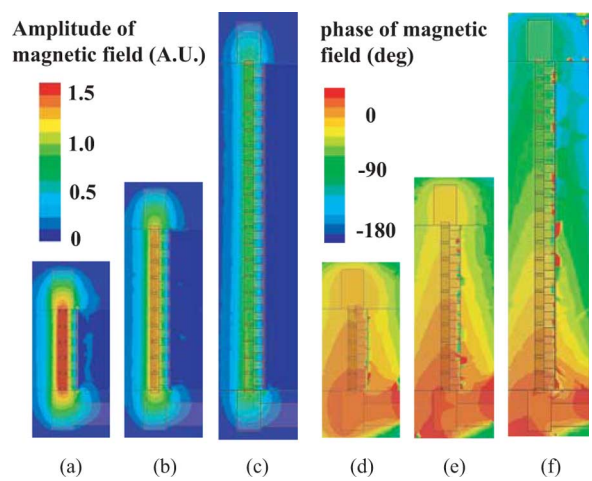

Fig. 8. (a)–(c) Simulated magnetic field profiles on the ground plane showing magnitude of current flow on the resonator as a function of the number of unit cells. Magnitude with: (a) five cells, (b) ten cells, and (c) 20 cells. (d)–(f) Corresponding phase profiles.

relatively stable with small variation from 6.12 to 6.19 GHz against the change in the externally applied dc magnetic field from −55 mT through zero to 34.5 mT in the linearly varying magnetization region. Measured relative bandwidth is almost constant with 2%, while the simulated result was 2.4%.

The influence of number of unit cells on the resonant conditions of pseudo-traveling-wave resonator is numerically investigated. Fig. 8 depicts simulated magnetic field profiles on the ground plane of the resonator showing how well confined the fields inside the resonator are for the number of cells with $N = 5,\ 10$ and 20. For short-ended resonance, series resonance in the series branch in the CRLHTL is dominant, and the current flow on the center microstrip line is significant. It is noted that the resonant condition in the present case satisfies the condition of leaky-wave radiation from the line. Therefore, the influence of leaky-wave radiation is more significant for larger number of cells in the resonators. It is confirmed from Fig. 8(a)–(c) that magnitude distribution is almost uniform along the resonator and that the resonator with a smaller number of cells has better confinement of the fields in the CRLH section. On the other hand, the phase gradient along the resonator is kept the same, independently of the number of cells in the resonators, as seen from Fig. 8(d)–(f). This result agrees well with predicted current distribution in (7).

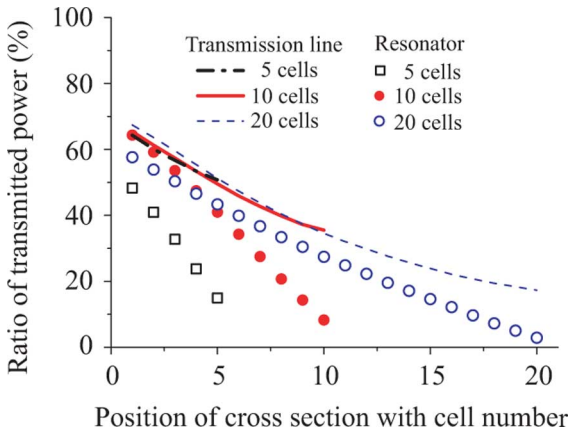

Fig. 9. Simulated power distribution along the nonreciprocal CRLHTL and the resonator, as a function of number of unit cells.

The transmitted power flow distribution along the resonator is also numerically investigated. We calculated the total power flow across designated areas that are the same as transverse cross section of the substrate region including a ferrite rod and dielectric substrates on both sides. Therefore, the simulation results neglect part of the power flow transmitting in the air region. Another power flow for the nonreciprocal CRLHTL without reflectors is also calculated for comparison. The simulation results are shown in Fig. 9 as a function of the position along the resonators and transmission lines. In the present case, the fields significantly decay along the line due to leaky-wave radiation from the line designed for antenna application to be mentioned later. It is noted that power flow at the terminal of the CRLH section for the resonators vanishes due to the cancellation of incident and reflected waves, whereas the transmission lines without reflectors do not. The cancellation of the transmitted power flow is more clearly observed for smaller number of unit cells. Indeed, there exists net power flow on the resonators near the input port, due to insufficient cancellation with superposition of exponential functions. The power distribution approaches that of transmission lines as the resonator's size becomes larger. It implies that a larger resonator has less confinement of fields resulting in conventional leaky-wave antennas without reflectors. This result is explained by the analytic approach in (9).

III. Application to Magnetically Tunable Beam-Steering Antennas

In this section, the proposed resonator is implemented into beam-steering antennas. As mentioned in Section II, the designed CRLHTL and the resonator showed significant leaky-wave radiation. The radiation angle from the leaky-wave transmission line can be roughly estimated from phase gradient of the field profile on the line, which is determined by the nonreciprocal phase at the intersection in the dispersion curves with $\beta = \beta_{\mathrm{NR}}$. The angle θ is measured with respect to broadside, as shown in Fig. 6(b), and is given by

$$\theta = \sin^{-1}\left(\frac{\beta}{\beta_0}\right) \tag{10}$$

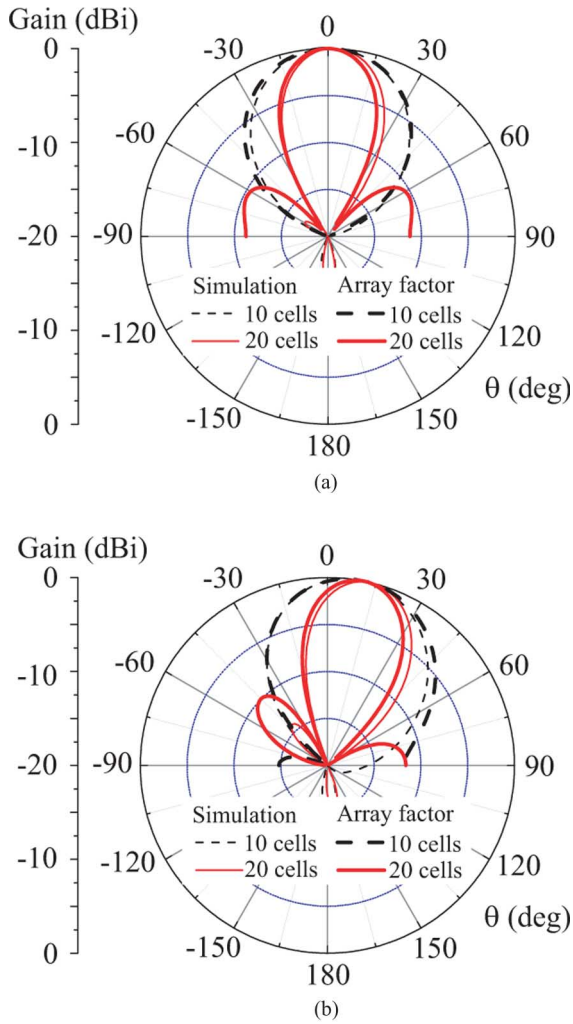

Fig. 10. Comparison of radiation patterns between numerical simulations and array factors, as a function of number of unit cells. (a) Without dc field with $\beta_{\mathrm{NR}} = 0$. (b) $B_{\mathrm{ext}} = 34.5$ mT with $\beta_{\mathrm{NR}} p/\pi = 0.025$.

where β_0 is the phase constant in free space. In order to analytically achieve radiation patterns from the current distribution along the resonator, the array factor can be formulated with the help of (1) as

$$R(\theta) = \sum_{n=1}^{N} I_n^+ e^{j(n-1)\beta_0 p \sin\theta + j\xi_n^+} + \sum_{n=1}^{N} I_n^- e^{j(n-1)\beta_0 p \sin\theta + j\xi_n^-} \tag{11}$$

with

$$\begin{aligned} I_n^+ &= I_0 e^{-\alpha_+(n-N)p} \\ I_n^- &= I_0 e^{\alpha_-(n-N)p} \\ \xi_n^+ &= -(n-N)\beta_+ p \\ \xi_n^- &= (n-N)\beta_- p. \end{aligned} \tag{12}$$

The normalized radiation patterns obtained from array factors using a propagation constant estimated from simulated dispersion curves are shown in Fig. 10 with thick lines along with

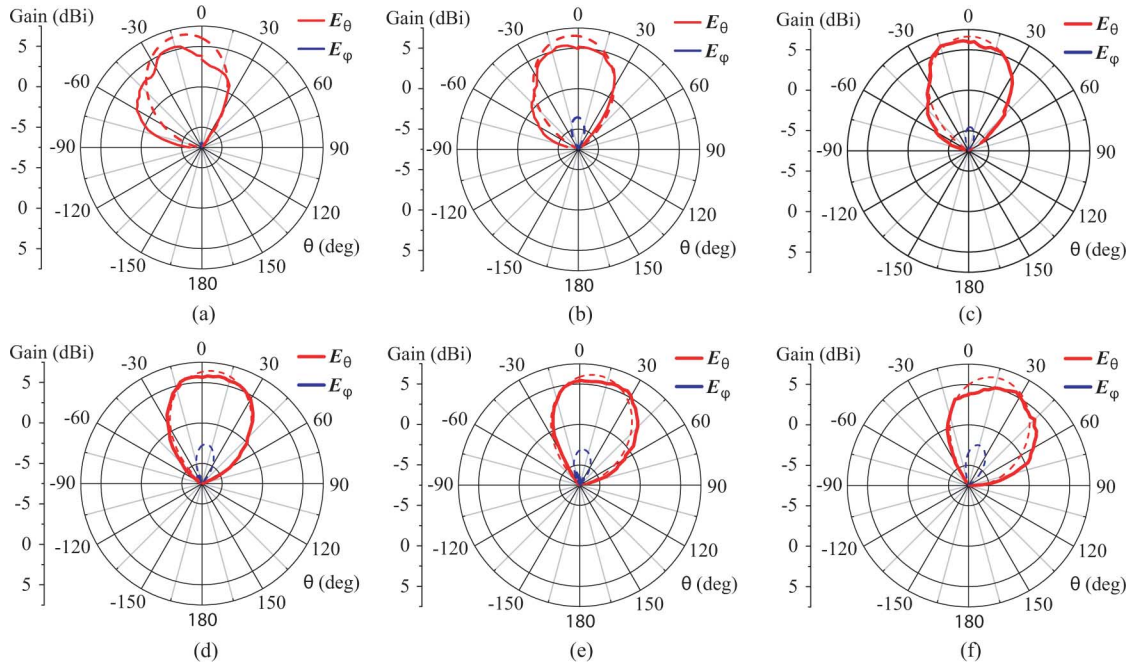

Fig. 11. Measured radiation patterns as a function of the external dc magnetic field. (a) $B_{\rm ext} = -55$ mT. (b) $B_{\rm ext} = -23$ mT. (c) $B_{\rm ext} = 0$ mT. (d) $B_{\rm ext} = 21.7$ mT. (e) $B_{\rm ext} = 34.5$ mT. (f) $B_{\rm ext} = 110$ mT.

radiation patterns directly obtained by numerical simulation with thin lines, as a function of the number of unit cells. Fig. 10(a) shows the no dc magnetic field case, or radiation from the zeroth-order resonator antenna, and the beam directs to broadside with the angle $\theta = 0$. Fig. 10(b) denotes the case with a dc field of $B_{\rm ext} = 34.5$ mT, which corresponds to a nonreciprocal phase with $\beta_{\rm NR}p/\pi = 0.025$. The angle was $\theta = 10^\circ$ for $N = 10$ and $\theta = 12^\circ$ for $N = 20$. For both cases with/without dc magnetic fields, the attenuation constants $\alpha_+ = \alpha_- = 0.3$ dB per unit cell are assumed, which are obtained from simulated transmission characteristics of the ten-cell CRLHTL in Fig. 3. It is noted that radiation patterns estimated from array factors in Fig. 10 have been modified by taking into account additional leaky-wave radiation from current distribution on the reflectors, which is composed of an open-end quarter-wavelength microstrip line and inserted at both sides of CRLH section, which results in enhancement of the effective antenna size and narrower beamwidth. Still, the enhancement of directivity with an increase in the number of the cells is clearly confirmed from Fig. 10. The simulated gain for $N = 10$ was 6.35 dBi, and 7.7 dBi for $N = 20$. Thus, the analytical approach based on array factors is in good agreement with the numerical simulation results for a different numbers of cells and a different degree of nonreciprocity.

In Fig. 11, measured radiation patterns are shown with solid lines as a function of the externally applied dc magnetic field from -55 to $+110$ mT. The simulated radiation patterns are also plotted with broken lines. It is noted that for the short-ended resonator, the series resonance in the series branch in the ladder network for the equivalent-circuit model of the nonreciprocal CRLHTL section is dominant [36], in a similar manner to conventional zeroth-order resonators [1]. The current distribution is then concentrated on the center microstrip line contributing

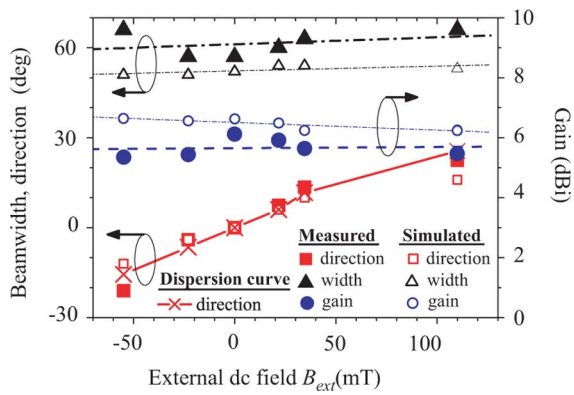

Fig. 12. Simulated and measured beam angles, beamwidth, and gains, as a function of the external dc magnetic field.

to the series branch. Therefore, co-polarized radiation mainly has the θ component of the electric fields, and the ϕ component is in cross-polarization. For negative dc field, effective magnetization in the ferrite rod becomes negative and nonreciprocal phase difference $\beta_{\rm NR}$ is also negative. On the other hand, the effective magnetization and the phase difference $\beta_{\rm NR}$ are both positive for the positive applied dc field, as shown in Figs. 3 and 4. The measured beam angle was continuously scanned from $\theta = -15^\circ$ to $\theta = 30^\circ$ with the variation of the external dc field restricted by the measurement setup. The simulated scanning angle of the antenna covers $\pm 30^\circ$.

In Fig. 12, measured and simulated beam angles, beamwidths, and radiation gains are shown as a function of the externally applied dc magnetic field. The beam angles estimated from (10) with the help of dispersion curves in Fig. 3 is also plotted for comparison. It is found from Fig. 12 that the simulated and measured beam angles, as well as a prediction

TABLE I
COMPARISON OF SIMULATED RADIATION EFFICIENCIES BETWEEN CRLHTL AND PSEUDO-TRAVELING-WAVE RESONATOR ANTENNAS

5 cells				
Structure	CRLHTL		Resonator antenna	
Ext. DC field (mT)	0	34.5	0	34.5
Center freq (GHz)	6.08	6.12	6.12	6.12
Return loss (%)	4.8	5.3	12.4	13.8
Efficiency (%)	17.4	16.6	83.8	80.7

10 cells				
Structure	CRLHTL		Resonator antenna	
Ext. DC field (mT)	0	34.5	0	34.5
Center freq. (GHz)	6.09	6.10	6.15	6.15
Return loss (%)	0.9	1.5	0.8	8.4
Efficiency (%)	41.2	41.1	95.2	85.5

20 cells				
Structure	CRLHTL		Resonator antenna	
Ext. DC field (mT)	0	34.5	0	34.5
Center freq. (GHz)	6.10	6.12	6.20	6.24
Return loss (%)	3.1	1.6	2.4	5.2
Efficiency (%)	69.7	67.9	93.7	89.7

from dispersion curves in Fig. 3, are all approximately proportional to the external dc field within the small magnitude of less than 50 mT. On the other hand, the simulated and measured gains were constantly about 6 and 5.5 dBi, respectively. The simulated and measured beamwidths were also stable with 50° and 60°, respectively. When the dc field is further enhanced and the effective magnetization approaches the saturation, the increase in the nonreciprocal phase $\beta_{\rm NR}$ is also saturated, as seen from Fig. 12.

Finally, advantages of the proposed antenna will be mentioned. First of all, it has considerably high radiation efficiency. Fundamental mechanism of leaky-wave radiation from the resonator antenna is the same as conventional leaky-wave antennas, but the efficiency is significantly improved by using multiple reflections at both ends. In Table I, comparison of radiation efficiencies between the proposed resonator antenna and the one-way propagation along the same CRLHTL is shown as a function of the number of unit cells. The radiation efficiency for conventional one-way propagation along the CRLHTL is enhanced by increasing the total length of the antennas. The efficiencies for both cases with and without dc fields are approximately the same with each other, and only 17% for five cells, and about 70% for 20 cells. The radiation efficiencies of the proposed resonator antennas in Table I seem to be varied with different number of unit cells. However, the variation is mainly due to different return losses by using the same reflectors as the ten-cell case. For example, when the matching condition is well achieved for the five-cell case with another optimized reflectors, the efficiency without a dc field was improved up to 95.4% and the one for a dc field with $B_{\rm ext} = 34.5$ mT was still 93.7%, as can be predicted from Table I, but the center frequency went down to 5.98 GHz. Of course, in these numerical simulation results, conductor loss, dielectric loss, as well as relatively large magnetic loss for polycrystalline YIG in the antennas have been taken into account.

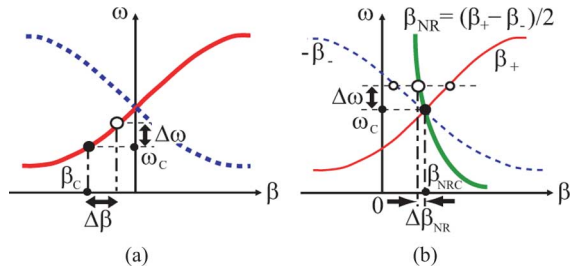

Fig. 13. Schematic of influence of modulated signals on the beam angles. (a) Conventional CRHLTL-based LWA. (b) Proposed pseudo-traveling-wave-resonator antenna.

The second advantage of the antenna is robust stability of steering beam direction against perturbation of the operational frequency or modulation of incident signals. For conventional CRLHTL-based leaky-wave antennas, beam direction is vulnerable to perturbation of the operational frequency $\Delta\omega$. We take the center frequency ω_C and the phase constant β_C, as shown in Fig. 13(a). The perturbation of beam direction $\Delta\theta$ can be derived from (10) and is given in terms of perturbation of the frequency $\Delta\omega$ by [39]

$$\Delta\theta \cong \frac{\Delta\omega}{\sqrt{\beta_0^2-\beta_C^2}}\left(\left.\frac{d\beta}{d\omega}\right|_{\omega=\omega_C}-\frac{\beta_C}{\omega_C}\right) = \frac{\Delta\omega}{\sqrt{\beta_0^2-\beta_C^2}}\left(\frac{1}{v_g}-\frac{1}{v_p}\right) \tag{13}$$

where $v_g = d\omega/d\beta|_{\omega=\omega_C}$, $v_p = \omega_C/\beta_C$. A factor $1/\sqrt{\beta_0^2-\beta_C^2}$ in (13) slowly varies with the operational frequency and is relatively constant, except for frequencies in the vicinity of singular points $\beta_C = \beta_0$ at the edge of the radiation region. Therefore, $\Delta\theta$ is almost proportional to another factor of a difference between reciprocal of the group velocity v_g and that of phase velocity v_p. In the fast wave region where leaky waves can be radiated, the phase velocity v_p exceeds a speed of light in vacuum c, whereas the group velocity v_g is less than c. Therefore, $\Delta\theta$ essentially remains finite. Still, it was successfully reduced by designing the CRLHTL with less dispersion and by selecting the operational frequency in the RH band near the air line [39]. However, especially for cases at frequencies in the vicinity of the intersection of dispersion curves, the fluctuation $\Delta\theta$ becomes significant and is approximately proportional to $1/v_g$ because $1/v_p$ is nearly zero with $\beta \cong 0$.

On the other hand, the proposed antenna is basically resonant-type and the beam direction is much more robust against the perturbation of the frequency, compared to conventional leaky-wave antennas. In order to estimate perturbation of the beam angle, phase gradient of the current distribution on the resonator needs to be formulated. The current distribution $I(x)$ in (1) is proportional to $g(x) = [e^{-\gamma_+(x-l)} + \Gamma_{c2}e^{\gamma_-(x-l)}]$. Under the assumption of $\Gamma_{C2} \sim 1$ and $\alpha_+(\omega) = \alpha_-(\omega)$, the factor is expressed by

$$g(x) = \sqrt{\cosh^2[\alpha_+(x-l)] - \sin^2[(\beta_+ - \beta_{\rm NR})(x-l)]} \times e^{-j[\beta_{\rm NR}(x-l)-\Delta\phi(x)]} \tag{14}$$

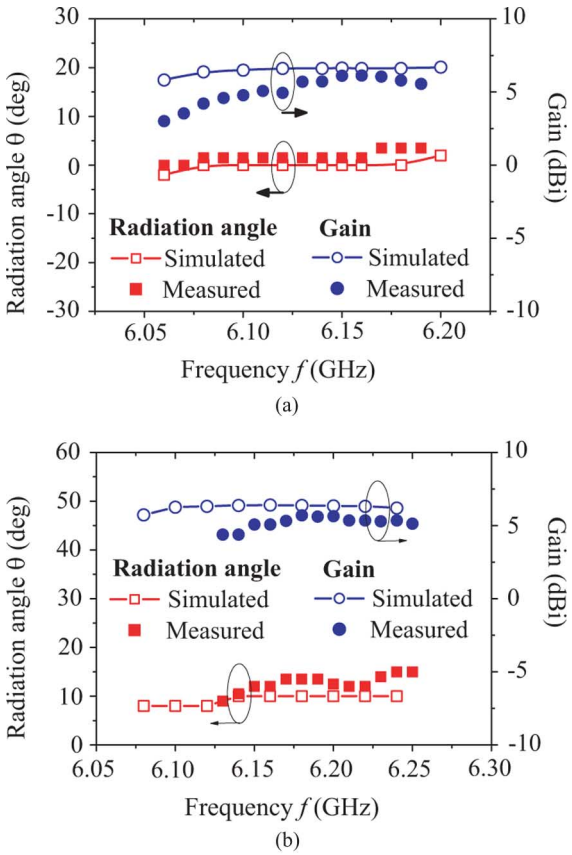

Fig. 14. Frequency dependence of simulated and measured radiation angles and gains. (a) Without dc field. (b) $B_{\rm ext} = 34.5$ mT.

with $\beta_{\rm NR} = (\beta_+ - \beta_-)/2$ and

$$\Delta\phi(x) = \tan^{-1}\left[\tanh\left\{\alpha(x-l)\right\}\cdot\tan\left\{(\beta_+ - \beta_{\rm NR})(x-l)\right\}\right] \cong \alpha_+(\beta_+ - \beta_{\rm NR})(x-l)^2. \quad (15)$$

It is found from (14) that the nonuniform magnitude is significant when either $|\alpha_+ l| \ll 1$ or $|(\beta_+ - \beta_{\rm NR})l| \ll 1$ is not satisfied, where the factor $(\beta_+ - \beta_{\rm NR})$ denotes the offset phase constant at the operational frequency, as shown in Fig. 13(b). The second term in phase of $g(x)$ in (14), $\Delta\phi(x)$ defined by (15), may generate nonlinearly varying phase distribution along the resonator. The nonlinearity in phase significantly appears when neither $|\alpha_+ l| \ll 1$, nor $|(\beta_+ - \beta_{\rm NR})l| \ll 1$ holds. In the present case, $|\Delta\phi(x)|$ is very small compared to the first term and can be neglected. Therefore, the perturbed beam angle is given in terms of $\beta_{\rm NR}$ and the perturbation $\Delta\omega$ by

$$\Delta\theta \cong \frac{\Delta\omega}{\sqrt{\beta_0^2 - \beta_{\rm NRC}^2}}\left(\left.\frac{d\beta_{\rm NR}}{d\omega}\right|_{\omega=\omega_C} - \frac{\beta_{\rm NRC}}{\omega_C}\right). \quad (16)$$

where $\beta_{\rm NRC}$ in (16) denotes the phase nonreciprocity at the center frequency, $\beta_{\rm NR}(\omega_C)$, as illustrated in Fig. 13(b). From (16), the perturbation of beam angle for the proposed antenna is approximately proportional to a factor of the difference between the first derivative of the phase nonreciprocity with respect to the frequency and the ratio of phase nonreciprocity to the frequency. In the present case with $B_{\rm ext} = 34.5$ mT, the derivatives of the phase nonreciprocity for simulated and measured results are both $d\beta_{\rm NR}/d\omega \cong -1 \times 10^{-9}$ s/m, and they are much smaller than the group delay of the same CRLH modes with $d\beta_\pm/d\omega \cong \pm 2 \times 10^{-8}$ s/m in (13) by a factor of 1/20. The second term $\beta_{\rm NRC}/\omega$ in parentheses of (16) is less than the first term. Thus, the robustness of the beam directions against modulated signals for the proposed resonator antenna is verified by the mechanism of the leaky-wave radiation and the nonreciprocal dispersion diagram. It should be emphasized that for the proposed pseudo-traveling-wave resonator antennas, the beam squinting can be drastically reduced without any additional efforts and could be set to precisely zero if the nonreciprocal dispersion is optimally designed, as predicted from (16).

In Fig. 14, frequency dependence of measured and simulated radiation angles and gains are shown within the -10-dB bandwidths for two cases with and without external dc magnetic fields. In the numerical simulation, both the frequency dependences of radiation angle and gain are found very small, which implies that the proposed antenna has very promising potential for use in communication applications, where modulated signals must be treated. In the measurement, there exist frequency dependences to some extent, but the essential results have been achieved.

IV. Conclusion

A pseudo-traveling-wave resonator with magnetically tunable phase gradient of field distribution has been investigated, and a new type of beam-steering antenna based on the resonator has been experimentally demonstrated for the first time. It is a short-ended transmission-line resonator and is composed of a nonreciprocal phase-shift CRLHTL using a polycrystalline YIG rod. The resonator operates as zeroth-order resonator if there is no dc magnetic field, and the radiation beam directs to broadside. By increasing an externally applied dc magnetic field normal to the substrate, the effective dc magnetization in the ferrite increased under the unsaturated region. The phase gradient of the field distribution along the resonator was then continuously increased. As a result, the radiation beam direction changed obliquely with respect to broadside. Continuous backfired-to-endfire beam steering with more than 40° was achieved with almost constant gain of 5 dBi. In addition, numerical simulation results showed considerably high radiation efficiency of 85%–95%, and the beam angle and gain were found almost constant within the relative bandwidth of 2%. The proposed resonator will open up new applications to compact and high-efficient beam-steering antennas in wireless communications.

Acknowledgment

The authors would like to thank Y. Tanaka, Orient Microwave Corporation, Shiga, Japan, for his supply of the ferrite bulk, and J. Noda, Kyoto Prefectural Technology Center for Small and Medium Enterprises, Kyoto, Japan, for his support of antenna measurement.

References

[1] A. Sanada, C. Caloz, and T. Itoh, "Zeroth-order resonance in composite right/left handed transmission line resonators," in *Proc. Asia–Pacific Microw. Conf.*, 2003, pp. 1588–1592.

[2] C. Caloz and T. Itoh, *Electromagnetic Metamaterials: Transmission Line Theory and Microwave Applications*. Hoboken, NJ: Wiley, 2006.
[3] G. V. Eleftheriades and K. G. Balmain, *Negative-Refraction Metamaterials: Fundamental Principles and Applications*. Piscataway, NJ: IEEE Press, 2005.
[4] A. Lai, C. Caloz, and T. Itoh, "Composite right/left-handed transmission line metamaterials," *IEEE Microw. Mag.*, vol. 5, no. 3, pp. 34–50, Sep. 2004.
[5] S. B. Cohn, "Parallel-coupled transmission-line-resonator filters," *IEEE Trans. Microw. Theory Tech.*, vol. MTT-6, no. 2, pp. 223–231, Apr. 1958.
[6] M. Antoniades and G. V. Eleftheriades, "A broadband series power divider using zero-degree metamaterial phase-shifting lines," *IEEE Microw. Wireless Compon. Lett.*, vol. 15, no. 11, pp. 808–810, Nov. 2005.
[7] A. Lai, K. M. K. H. Leong, and T. Itoh, "A novel N-port series divider using infinite wavelength phenomena," in *IEEE MTT-S Int. Microw. Symp. Dig.*, Jun. 2005, Paper WE4E-5.
[8] A. Sanada, M. Kimura, I. Awai, C. Caloz, and T. Itoh, "A planar zeroth-order resoqnator antenna using a left-handed transmission line," in *Proc. 34th Eur. Microw. Conf.*, Sep. 2004, pp. 1341–1344.
[9] A. Lai, K. M. K. H. Leong, and T. Itoh, "Infinite wavelength resonant antennas with monopolar radiation pattern based on periodic structures," *IEEE Trans. Antennas Propag.*, vol. 55, no. 3, pp. 868–876, Mar. 2007.
[10] J.-G. Lee and J.-H. Lee, "Zeroth-order resonance loop antenna," *IEEE Trans. Antennas Propag.*, vol. 55, no. 3, pp. 994–997, Mar. 2007.
[11] C. Caloz, T. Itoh, and A. Rennings, "CRLH metamaterial leaky-wave and resonant antennas," *IEEE Antennas Propag. Mag.*, vol. 50, no. 5, pp. 25–39, Oct. 2008.
[12] T. Yoshida, T. Ueda, M. Akiyama, and T. Itoh, "Radiation characteristics of zeroth-order resonators composed of 2-D dielectric-based composite right/left handed metamaterial structures," in *Proc. 39th Eur. Microw. Conf.*, Sep. 2009, pp. 205–208.
[13] S. Pyo, S.-M. Han, J.-W. Baik, and Y.-S. Kim, "A slot-loaded composite right/left-handed transmission line for a zeroth-order resonant antenna with improved efficiency," *IEEE Trans. Microw. Theory Tech.*, vol. 57, no. 11, pp. 2775–2782, Nov. 2009.
[14] T. Ueda, G. Haida, and T. Itoh, "Zeroth-order resonators with variable reactance loads at both ends," *IEEE Trans. Microw. Theory Tech.*, vol. 59, no. 3, pp. 612–618, Mar. 2011.
[15] T. Ueda, G. Haida, Y. Kado, and T. Itoh, "Polarization-controllable zeroth-order-resonator antennas with reactance loads at both ends," in *IEEE MTT-S Int. Microw. Symp. Dig.*, Jun. 2011, pp. 1–4, Paper TU2F-2.
[16] T. Grbic and G. V. Eleftheriades, "A backward-wave antenna based on negative refractive index *L–C* networks," in *IEEE AP-S Int. Symp. Dig.*, Jun. 2002, vol. 4, pp. 340–343.
[17] T. Grbic and G. V. Eleftheriades, "Experimental verification of backward-wave radiation from a negative refractive index metamaterial," *J. Appl. Phys.*, vol. 92, no. 10, pp. 5930–5935, Nov. 2002.
[18] L. Liu, C. Caloz, and T. Itoh, "Dominant mode (DM) leaky-wave antenna with backfire-to-endfire scanning capability," *Electron. Lett.*, vol. .38, no. 23, pp. 1414–1416, Nov. 2002.
[19] F. C. Miranda, C. C. Penalosa, and C. Caloz, "High-gain active composite right/left-handed leaky-wave antenna," *IEEE Trans. Antennas Propag.*, vol. 54, no. 8, pp. 2292–2300, Aug. 2006.
[20] T. Ueda, N. Michishita, M. Akiyama, and T. Itoh, "Dielectric-resonator- based composite right/left-handed transmission lines and their application to leaky wave antenna," *IEEE Trans. Microw. Theory Tech.*, vol. 56, no. 10, pp. 2259–2268, Oct. 2008.
[21] T. Ikeda, K. Sakakibara, T. Matsui, N. Kikuma, and H. Hirayama, "Beam-scanning performance of leaky-wave slot-array antenna on variable stub-loaded left-handed waveguide," *IEEE Trans. Antennas Propag.*, vol. 56, no. 12, pp. 3611–3618, Dec. 2008.
[22] S. Paulotto, P. Baccarelli, F. Frezza, and D. Jackson, "Full-wave modal dispersion analysis and broadside optimization for a class of microstrip CRLH leaky-wave antennas," *IEEE Trans. Microw. Theory Tech.*, vol. 56, no. 12, pp. 2826–2837, Dec. 2008.
[23] Y. Dong and T. Itoh, "Composite right/left-handed substrate integrated waveguide and half mode substrate integrated waveguide leaky-wave structures," *IEEE Trans. Antennas Propag.*, vol. 59, no. 3, pp. 767–775, Mar. 2011.
[24] S. Lim, C. Caloz, and T. Itoh, "Metamaterial-based electronically controlled transmission line structure as a novel leaky-wave antenna with tunable angle and beamwidth," *IEEE Trans. Microw. Theory Tech.*, vol. 53, no. 1, pp. 161–173, Jan. 2005.
[25] H. V. Nguyen, S. Abielmona, and C. Caloz, "Highly efficient leaky-wave antenna array using a power-recycling series feeding network," *IEEE Trans. Antennas Wireless Propag. Lett.*, vol. 8, pp. 441–444, Jun. 2009.
[26] H. V. Nguyen, A. Parsa, and C. Caloz, "Power-recycling feedback system for maximization of leaky-wave antennas' radiation efficiency," *IEEE Trans. Microw. Theory Tech.*, vol. 58, no. 7, pp. 1641–1650, Jul. 2010.
[27] C.-T. M. Wu, Y. Dong, J. S. Sun, and T. Itoh, "Ring-resonator-inspired power recycling scheme for gain-enhanced distributed amplifier-based CRLH-transmission line leaky wave antennas," *IEEE Trans. Microw. Theory. Tech.*, vol. 60, no. 4, pp. 1027–1037, Apr. 2012.
[28] M. Tsutsumi and T. Ueda, "Nonreciprocal left-handed microstrip lines using ferrite substrate," in *IEEE MTT-S Int. Microw. Symp. Dig.*, Jun. 2004, pp. 249–252.
[29] T. Ueda and M. Tsutsumi, "Nonreciprocal left-handed transmission characteristics of microstrip lines on the ferrite substrate," *IET Microw., Antennas, Propag.*, vol. 1, no. 2, pp. 349–354, Apr. 2007.
[30] T. Ueda and M. Tsutsumi, "Left-handed transmission characteristics of ferrite microstrip lines without series capacitive load," *IEICE Trans. Electron.*, vol. E89-C, no. 9, pp. 1318–1323, Sep. 2006.
[31] T. Ueda, K. Horikawa, M. Akiyama, and M. Tsutsumi, "Nonreciprocal phase-shift composite right/left handed transmission lines and their application to leaky wave antennas," *IEEE Trans. Antennas Propag.*, vol. 57, no. 7, pp. 1995–2005, Jul. 2009.
[32] T. Ueda, "Transmission line microwave apparatus including at least one non-reciprocal transmission line part between two parts," U. S. Patent App. Pub. US 2010/0060388 A1, Mar. 11, 2010.
[33] T. Ueda and M. Akiyama, "Nonreciprocal phase-shift composite right/left handed transmission lines using ferrite-rod-embedded substrate," *IEEE Trans. Magn.*, vol. 45, no. 10, pp. 4203–4206, Oct. 2009.
[34] H. Kishimoto, T. Ueda, and Y. Kado, "Experimental demonstration of nonreciprocal phase-shift composite right/left handed transmission lines using a ferrite-rod-embedded substrate," *IEEE Trans. Magn.*, vol. 47, no. 10, pp. 3724–3727, Oct. 2011.
[35] K. Horikawa, T. Ueda, and M. Akiyama, "Influence of reflected waves at a terminal of nonreciprocal phase-shift CRLH transmission lines on the leaky wave radiation," in *Proc. Asia–Pacific Microw. Conf.*, Dec. 7–10, 2009, pp. 151–154.
[36] T. Ueda and H. Kishimoto, "Pseudo-traveling wave resonator based on nonreciprocal phase-shift composite right/left handed transmission lines," in *IEEE MTT-S Int. Microw. Symp. Dig.*, May 2010, pp. 41–44.
[37] T. Ueda, S. Yamamoto, and Y. Kado, "Beam-scanning traveling-wave-resonator antenna based on nonreciprocal phase-shift CRLH transmission lines," in *Proc. IEEE Int. Antennas Propag. Symp.*, Jul. 2011, pp. 1058–1061.
[38] K. Horikawa, T. Ueda, and M. Akiyama, "Beam steering of leaky wave radiation from nonreciprocal phase-shift composite right/left handed transmission lines," *IEICE Trans. Electron.*, vol. E93-C, no. 7, pp. 1089–1097, Jul. 2010.
[39] M. A. Antoniades and G. V. Eleftheriades, "A CPS leaky-wave antenna with reduced beam squinting using NRI-TL metamaterials," *IEEE Trans. Antennas Propag.*, vol. 56, no. 3, pp. 708–721, Mar. 2008.

Tetsuya Ueda (M'97–SM'10) received the B.E., M.E., and Ph.D. degrees in communication engineering from Osaka University, Osaka, Japan, in 1992, 1994, and 1997, respectively.

Since 1997, he has been with the Department of Electronics, Kyoto Institute of Technology, Kyoto, Japan, where he is currently an Assistant Professor. From 2005 to 2006, he was a Visiting Scholar with the Department of Electrical Engineering, University of California at Los Angeles (UCLA). His current research interests include metamaterials and their applications.

Dr. Ueda is a member of the Institute of Electronics, Information and Communication Engineers (IEICE), Japan. He was the recipient of the 1999 IEICE Young Engineer Award and the 2008 IEEE MTT-S Japan Chapter Young Engineer Award.

Shintaro Yamamoto received the B.E. and M.E. degrees in electronics from the Kyoto Institute of Technology, Kyoto, Japan, in 2010 and 2012, respectively.

His research interests include metamaterials and their antenna applications.

Yuichi Kado (M'08) received the M.S. and Ph.D. degrees in electronics from Tohoku University, Miyagi, Japan, in 1983 and 1998, respectively.

In 1983, he joined the Electrical Communication Laboratories, Nippon Telegraph and Telephone Public Corporation (now NTT), Kanagawa, Japan, where he was engaged in research on silicon-on-insulator (SOI) structure formation by hetero-epitaxial growth. From 1989 to 1998, he was involved with the development of fully depleted CMOS/SIMOX large-scale integrations (LSIs) and ultra-low-power CMOS circuits. From 1999 to 2002, he was engaged in research and development on compact network appliances using ultra-low-power CMOS circuit technologies for ubiquitous communications. He led research and development projects on ultra-low-power network appliances, sub-terahertz-wave wireless communication, and intra-body communication as a Director of the Smart Devices Laboratory, NTT Microsystem Integration Laboratories (2003–2010). In July 2010, he joined the Department of Electronics, Kyoto Institute of Technology, Kyoto, Japan.

Dr. Kado was the recipient of the 2009 Nikkei BP Technology Award, the 2009 Radiowave Achievement Award presented by the Association of Radio Industries and Businesses (ARIB), and the 2011 Session's Best Paper Award presented by the International Institute of Informatics and Systemics (IIIS).

Tatsuo Itoh (S'69–M'69–SM'74–F'82–LF'06) received the Ph.D. degree in electrical engineering from the University of Illinois at Urbana-Champaign, in 1969.

After working for University of Illinois, SRI, and University of Kentucky, he joined the faculty of The University of Texas at Austin in 1978, where he became a Professor of electrical engineering in 1981. In September 1983, he was selected to hold the Hayden Head Centennial Professorship of Engineering at The University of Texas at Austin. In January 1991, he joined the University of California at Los Angeles (UCLA), as a Professor of electrical engineering and Holder of the TRW Endowed Chair in Microwave and Millimeter Wave Electronics (currently Northrop Grumman Endowed Chair). He has authored or coauthored 400 journal publications, 820 refereed conference presentations, and 48 books/book chapters in the area of microwaves, millimeter-waves, antennas and numerical electromagnetics. He has generated 73 Ph.D. students.

Dr. Itoh is a member of the Institute of Electronics and Communication Engineers of Japan, and Commissions B and D, USNC/URSI. He was the editor-in-chief of the IEEE TRANSACTIONS ON MICROWAVE THEORY AND TECHNIQUES (1983–1985). He was president of the IEEE Microwave Theory and Techniques Society (IEEE MTT-S) (1990). He was the editor-in-chief of the IEEE MICROWAVE AND GUIDED WAVE LETTERS (1991–1994). He was the chairman of Commission D, International URSI (1993–1996). He serves on Advisory Boards and committees of a number of organizations. He was a Distinguished Microwave Lecturer on Microwave Applications of Metamaterial Structures of the IEEE MTT-S (2004–2006). He was the recipient of a number of awards including the IEEE Third Millennium Medal (2000) and the IEEE MTT-S Distinguished Educator Award (2000). He was elected a member of the National Academy of Engineering in 2003. In 2011, he was the recipient of the Microwave Career Award of the IEEE MTT-S.